Enhancing discharge estimation from SWOT satellite data in a tropical tidal river environment

Francisco Rodrigues Do Amaral, Thierry Pellarin, Tin Nguyen Trung, Tran Anh Tu, Nicolas Gratiot

PLOS WATER

RESEARCH ARTICLE

Enhancing discharge estimation from SWOT satellite data in a tropical tidal river environment

Francisco Rodrigues do Amaral[1]*, Thierry Pellarin[1], Tin Nguyen Trung[2], Tran Anh Tu[2,3], Nicolas Gratiot[1,2]

1 Université Grenoble Alpes, CNRS, INRAE, IRD, Grenoble INP, IGE, Grenoble, France, **2** CARE, Ho Chi Minh City University of Technology (HCMUT), VNU-HCM, Ho Chi Minh City, Viet Nam, **3** Vietnam National University-Ho Chi Minh City (VNU-HCM), Thu Duc City, Ho Chi Minh City, Viet Nam

* francisco.amaral@univ-grenoble-alpes.fr

Citation: Rodrigues do Amaral F, Pellarin T, Trung TN, Anh Tu T, Gratiot N (2024) Enhancing discharge estimation from SWOT satellite data in a tropical tidal river environment. PLOS Water 3(2): e0000226. https://doi.org/10.1371/journal.pwat.0000226

Editor: Daniel Reddythota, Faculty of Water Supply & Environmental Engineering, ArbaMinch Water Technology Institute (AWTI), ETHIOPIA

Received: October 11, 2023

Accepted: January 10, 2024

Published: February 12, 2024

Peer Review History: PLOS recognizes the benefits of transparency in the peer review process; therefore, we enable the publication of all of the content of peer review and author responses alongside final, published articles. The editorial history of this article is available here: https://doi.org/10.1371/journal.pwat.0000226

Data Availability Statement: The in-situ data used in this study was acquired from the following open-

Abstract

The Surface Water and Ocean Topography (SWOT) mission aims to provide essential data on river width, height and slope in order to estimate worldwide river discharge accurately. This mission offers a powerful tool for monitoring river discharge in dynamic coastal areas, like the Saigon-Dongnai estuary in Southern Vietnam. However, estimating discharge of tidally-influenced rivers using SWOT measurements can be challenging when hydraulic variables have the same order of magnitude as SWOT measurement errors. In this paper we present a methodology to enhance discharge estimation accuracy from SWOT measurements based on simulated SWOT products at the 200 meter node resolution and varying river reach size. We assess measurement error variability and its impact on discharge estimation by employing a Monte Carlo analysis. Our approach significantly improved discharge estimation in the Saigon tidal river, reducing RMSE from 1400 m^3/s to 180 m^3/s and increasing R^2 from 0.31 to 0.95. Notably, the percentage of Monte Carlo particles meeting the 30% rRMSE threshold rose from 0% to 79%. This study underscores the feasibility of obtaining reliable discharge estimates from SWOT data in complex coastal areas where hydraulic variables are of the same order of magnitude as SWOT errors. Additionally, the proposed methodology to improve discharge estimation from SWOT measurements is widely adaptable as it can be applied to similar regions and can be combined with any discharge estimation method.

1. Introduction

Geophysical processes occurring at the surface of the Earth in low elevation coastal zones (LECZs) are primarily regulated by the interplay of river discharge and the intricate dynamics imposed by the coastal ocean. Within this transitional zone, there exists a region often referred to as "the tidal river". This area is profoundly influenced by tidal movements, surges, and the variations in mean sea level but remains devoid of significant salinity. It is a stretch of the river that is impacted by these marine forcing processes, yet it has historically received relatively

access publication: https://www.sciencedirect.com/science/article/pii/S2352340923002664?via%3Dihub This data can be downloaded directly from the following public repository: https://dataverse.ird.fr/dataset.xhtml?persistentId=doi:10.23708/NKQDNB.

Funding: The authors received no specific funding for this work.

Competing interests: The authors have declared that no competing interests exist.

little attention from the geophysical research community [1]. Notably, these tidal river reaches can extend inland for hundreds of kilometers, and in the case of larger rivers, they often rival or surpass the estuary in terms of both length and sometimes even area. Predicting water levels in tidal rivers or estuaries is a challenge due to the highly variable flow conditions that characterize these environments. The hydrological dynamics within a tidal river are inherently distinct, marked by a constant flux in water levels driven by the interplay of hydro-meteo-marine phenomena. Consequently, the hydrodynamic processes governing tidal rivers defy simplification, showcasing traits such as complexity, non-stationarity, and nonlinear behavior [2].

Remote sensing observations play a pivotal role in providing information on the spatial variations of water surface elevations across diverse hydrodynamic scenarios. In the last two decades, satellite radar altimeters, which excel at gauging sea level fluctuations, have introduced significant advancements in our understanding of ocean dynamics [3, 4]. However, their utility has been notably impeded when applied to coastal environments, where data accuracy decreases as these instruments approach coastal regions. This limitation is further exacerbated by the inherent constraints of nadir altimetry missions, exemplified by missions like Topography Experiment/POSEIDON (TOPEX/POSEIDON) and the Jason series [5]. These missions grapple with challenges posed by inter-track spacing and temporal resolution, which curtail their ability to effectively observe smaller-scale coastal phenomena, including shelf tides, coastal tides, wind-induced effects, and storm surges [6]. A transformative shift in the landscape of coastal remote sensing is to be expected with the National Aeronautics and Space Administration/Centre National d'Études Spatiales (NASA/CNES) Surface Water and Ocean Topography (SWOT) satellite mission, launched on December 15th, 2022.

The SWOT satellite signifies a leap forward in our capacity to estimate global river discharge, substantially enriching our observational foundation for understanding worldwide hydrological phenomena [7]. River discharge measurements offer a comprehensive synthesis of upstream water cycle processes, rendering them indispensable data resources for gaining insights into hydrology across scales, from watershed dynamics to continental-scale patterns. Nonetheless, a substantial portion of the world's rivers remains unmonitored, owing to various constraints encompassing resource limitations and data sharing challenges [8, 9] especially in the inter-tropical zone [10]. Remote sensing techniques aimed at gauging river discharge hold the potential to extend global observation capabilities, even in regions lacking conventional gauging infrastructure. However, this expanded reach comes with trade-offs. Remote sensing methods generally entail compromises, encompassing reduced measurement precision, accuracy, and temporal sampling frequency when compared to in-situ discharge monitoring practices [11]. SWOT's capability of capturing parameters such as river water surface elevation (WSE) (also referred to simply as river water level), top width, and longitudinal water surface slope (also referred simply as slope) [12] enables estimations of river discharge.

The SWOT satellite, equipped with advanced radar altimetry technology and unprecedented spatial resolution, offers an innovative opportunity to quantify river discharge across the globe with unparalleled accuracy. However, harnessing SWOT data for discharge estimation requires comprehensive evaluation and optimization, particularly in complex hydrological settings such as tidal rivers. The SWOT team's objective for the coastal ocean is to "quantify the water exchanges between coastal regions, estuaries, deltas, and wetlands" [13]. It is in accordance with this objective that we propose an evaluation of the capability of future SWOT satellite measurements in estimating water discharge in the Saigon river situated in Southern Vietnam. The Saigon river is a tidal river located in a densely populated, highly complex LECZ. The study of the hydrodynamics and hydrology of the Saigon River is important in water resource management, flood control, and navigation in the Ho Chi Minh City (HCMC)

megalopolis. Nonetheless, this case study has the potential to be applied to other megalopolis sharing comparable human and geophysical environments.

Another reason for the interest in how SWOT satellite measurements can be used to estimate tidal river discharge is the alarming flood vulnerability in coastal and other low-lying cities [14]. In particular, HCMC is one of the most vulnerable cities in the world with respect to climate change [15]. Some of these vulnerabilities are water-related issues such as lack of urban services like drinking-water management, sanitation, rainwater drainage and compound flooding. Specifically, flooding vulnerability is linked to sea level rise, rainfall intensification, storm surges and ground subsidence while 65% of the city is located at less than 1.5 m above sea level. In addition, HCMC is home to almost 10 million inhabitants and its population grows at about 3% per year with these risks posing a threat to many livelihoods [15]. Several studies consider HCMC as a hotspot of vulnerability to climate change [16–21]. However, there has been little comprehensive studies regarding the potential of SWOT in an estuary setting such as the one in this study area. Furthermore, we suggest an innovative approach to simulate SWOT data and enhance its quality. This method is adaptable and can be applied to other intricate tidal river systems within dynamic coastal areas.

Given the accessibility of hydrological variables derived from SWOT, characterized by specific resolutions and accuracy thresholds, the scientific community has put forward multiple methodologies for estimating river discharge. These methodologies are constructed upon distinct assumptions and simplifications. For instance, Durand et al. 2016 [22] conducted a comparative analysis, evaluating the efficacy of five different algorithms that leverage SWOT-like observations in assessing flow rates across 19 major rivers. While this examination revealed that, in nearly every case (specifically, 14 out of 19 instances) at least one approach yielded satisfactory performance as indicated by a root mean square error below the 35% threshold, it underscores that achieving precise and dependable discharge estimation remains a topic of concern. However, SWOT capabilities for estuaries and tidal rivers have received comparatively little attention [5, 23, 24]. This calls for continued research efforts in the field to enhance the accuracy and reliability of these estimations, particularly in LECZs, a focus that this paper seeks to address.

In this paper we propose an original methodology to obtain high spatial resolution water level time-series directly from in-situ measurements. Then, we re-create SWOT-like measurements of water level and slope along the Saigon river, coupled with innovative reach size selection to estimate river discharge. Through an extensive analysis, we evaluate the performance of this methodology under various conditions, including reach sizes, discharge values, and error considerations. Our investigation explores the limitations of the expected SWOT-like discharge estimation errors and proposes an enhanced approach that leverages SWOT data more effectively. We assess the impact of reach size, a critical parameter in SWOT-based discharge estimation, on accuracy and computational efficiency. By conducting a Monte Carlo analysis, we scrutinize the sensitivity of discharge estimates to errors inherent in SWOT-like measurements [25, 26]. Ultimately, this research advances the broader goal of harnessing the potential of SWOT measurements to enhance our understanding of tidally forced riverine systems, contributing to improved water resource management and environmental conservation efforts in vulnerable LECZ.

2. Materials and methods

2.1. Study area description

The Saigon-Dongnai River system is located in Southern Vietnam (Fig 1). The Saigon river branch is a complex river system, subject to several human and environmental interactions

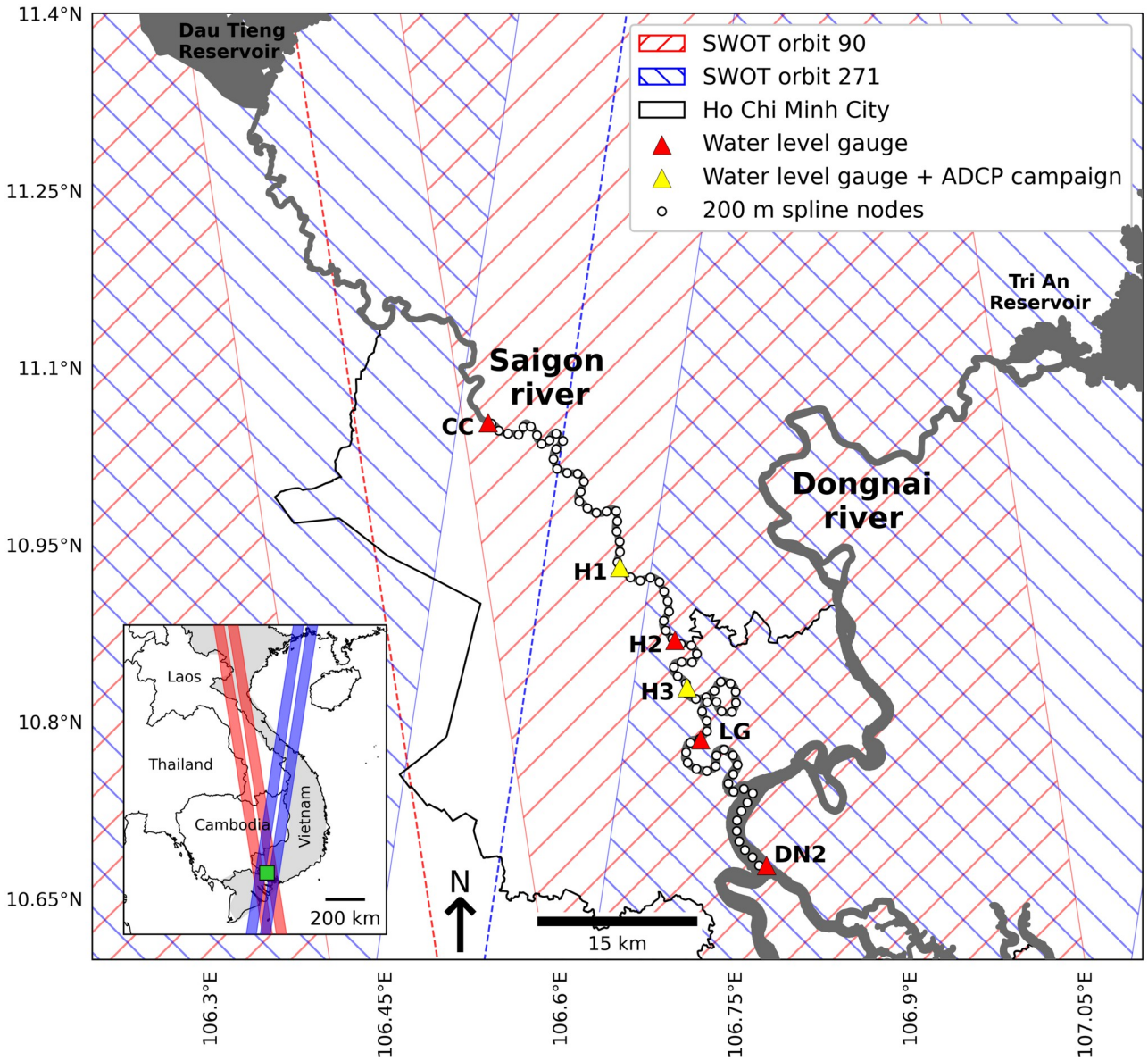

Fig 1. Map of the study area. The Saigon-Dongnai river system and the two SWOT satellite swaths (hatch pattern) and nadir lines (dotted line) that cover the area. The river is covered by both swaths in areas where the red and blue hatch patterns intersect and form squares. The water level gauges namely, Cu Chi (CC), Hobo 1 (H1), Hobo 2 (H2), Hobo 3 (H3), La Garden (LG) and Dongnai 2 (DN2) are shown as well as the ADCP campaign locations (triangles). The spline spatial interpolation nodes at every kilometer is illustrated as white dots. The area shown in the larger map is represented by the green box in the overview map. Basemap used in main map can be downloaded from www.igismap.com/vietnam-shapefile-download-country-boundaryline-polygon (under CC BY 3.0 IGO licence. For terms of use please see: https://map.igismap.com/terms-of-services). Basemap used in the overview map downloaded from www.naturalearthdata.com/downloads/10m-cultural-vectors/10m-admin-0-countries (public domain data see www.naturalearthdata.com/about/terms-of-use/ for the terms of use).

https://doi.org/10.1371/journal.pwat.0000226.g001

before flowing into the Dongnai River and finally, into coastal waters. It flows from its source in Cambodia to the Dau Tieng Reservoir (270 km^2 and 1,580 · 10^6 m^3) before passing through the HCMC megalopolis. In total, it is 225 km long and its catchment area has a surface of about 4,800 km^2. The Dau Tieng Reservoir was designed for flood control, water supply, and preventing saltwater intrusion [27, 28]. The hydrodynamics of the Saigon River are influenced

by various factors including tidal processes, freshwater inflows, and sediment transport. Tidal dynamics play the most significant role in shaping the river's behavior, with tidal amplitudes ranging from 1 (neap tide) to 4 meters (spring tide) [29] and water discharge ranging between -1500 m^3s^{-1} and 2000 m^3s^{-1}[30]. Tidal fluctuations dominate the totality of the river Saigon from the confluence with the Dongnai river to the outlet of the Dau Tieng reservoir. In fact, at the seasonal scale the river water levels are controlled by the coastal water levels [20].

The HCMC megalopolis, with a population of approximately 10 million inhabitants, is located along the banks of the Saigon River and is the largest and most densely populated city in Vietnam. The population is concentrated in the heart of the city, with the urban districts housing about 6.7 million inhabitants [31]. The city's rapid urbanization, economic development, and population growth have posed challenges including river pollution, flood risk, and wastewater management [32, 33].

2.2. Measurement campaign

A high-resolution dataset comprising water level measurements and Acoustic Doppler Current Profiler (ADCP) campaigns was collected during a 2-month field campaign conducted in the study region, as part of a collaborative effort between the Centre Asiatique de Recherche sur L'Eau (CARE, Vietnam) and the Institut des Géosciences de l'Environnement (IGE, France). The campaign was specifically designed to support the hydraulic study aimed at assessing the applicability of the SWOT satellite to the Saigon-Dongnai estuary system. The dataset includes water level measurements at six selected locations along the Saigon River, namely Cu Chi (CC), Hobo 1 (H1), Hobo 2 (H2), Hobo 3 (H3), La Garden (LG) and Dongnai 2 (DN2) (triangles in Fig 1). The selection of these locations was bound by on-site constraints (inaccessibility to the riverbank, challenges in sensor installation, among others) and aimed to align with two primary criteria: i. comprehensively covering key sections of the Saigon River, particularly within Ho Chi Minh City and immediately upstream, areas of significant societal interest and impact; and ii. maintaining a distance of approximately 10 km between sensors to emulate the spatial resolution of SWOT reach products.

These measurements were obtained by a submersed brick-and-pipe installation of Onset HOBO U20L-01 water level loggers measuring absolute pressure at a time resolution of 15 minutes. To ensure accuracy, the water level measurements were barometrically compensated using air pressure measurements. The vertical reference point of the pressure sensors is different and unknown. In order to be able to compare the signals at different locations, all signals are normalized [34]. Furthermore, we use a slope correction parameter in our discharge estimation method that is used to compensate for the fact that the reference points of each location are different and unknown (explained in Sect. 2.6). Additionally, discharge measurements were obtained through three 24-hour ADCP campaigns during both symmetric and asymmetric tidal regimes at two locations (yellow triangles in Fig 1). Despite its relatively short duration, the dataset provides unprecedented spatial and temporal resolution for water level and discharge measurements. The synchronous recording of multiple water level sensors along the river enables the study of water surface slope profiles. Furthermore, the concurrent discharge measurements facilitate the calibration of the discharge estimation law proposed in this paper. More detailed information on this dataset can be found in [34].

2.3. The SWOT mission

The SWOT mission, led by the National Aeronautics and Space Administration (NASA) and the French space agency (Centre National d'Études Spatiales, CNES), in collaboration with the Canadian and UK space agencies (CSA and UKSA, respectively), aims to contribute to the

fundamental understanding of the Earth system by providing high spatial resolution and global measurements for ocean and inland water. The launch of SWOT took place on December 16, 2022, and the mission is currently in the science phase. The first validated river products of water surface elevation (WSE), width, and slope are expected to be available in April 2024. The mission focuses on ocean and terrestrial water bodies including lakes, reservoirs, wetlands, and rivers, with specific criteria such as surface area exceeding 62,500 m^2 and rivers wider than 100 m, with the goal of potentially reaching 50 m [12, 35, 36]. The SWOT satellite's core payload includes a Ka-band radar interferometer (KaRIn) operating at a frequency of 35.75 GHz (wavelength of 8.6 mm) and with a near-nadir incidence angle [37].

In terms of spatial coverage and revisit time, the SWOT satellite aims to achieve near-global coverage between 78˚S and 78˚N with a revisit time of approximately 21 days. The satellite will employ radar observations with pixels of about 6 m in the azimuth direction and varying from 10 to 60 m in the direction perpendicular to the azimuth. To meet mission requirements for observation accuracy, averaging procedures will be applied to the radar data [7, 12, 38]. The resulting SWOT products will be available within two swaths of 50 km width, separated by a gap of 20 km known as the "nadir gap".

The SWOT mission's capabilities enable the measurement of water extent, water surface elevation, and slope, facilitating the estimation of river and global storage variation at sub-monthly, seasonal, and annual time scales [12]. The SWOT observations, with their finer spatial resolution, provide a global inventory of terrestrial water bodies, offering insights into lakes, reservoirs, wetlands, and rivers. The relative error for water-surface-area measurements is targeted to be less than 15% [9]. Additionally, SWOT products combined with hydraulic models or flow laws show potential to estimate instantaneous river discharge within 35% root-mean-square error [22].

The Saigon-Dongnai river system is monitored by two SWOT orbits: 90 and 271 (Fig 1 red and blue, respectively). This system will therefore receive two observations within the period of 21 days (i.e., satellite revisit time) namely, on day 4 (orbit 90) and day 10 (orbit 271). Together both orbits cover the entirety of the system at least once per 21 day period. The Saigon portion of the system is observed in an heterogeneous way in both space and time due to the nadir gaps on both orbits intercepting the river. Starting from the upstream Dau Tieng reservoir, the first 56 kms are observed on day 10; the section from kilometers 56 to 94 is observed on day 4 and the remaining section from kilometer 94 to the confluence with the Dongnai river is monitored on day 4 and 10. On the other hand, the Dongnai river is observed in its entirety by both orbits' right swaths.

The section of the Saigon river under scope extends from the CC water level gauge to the DN2 gauge downstream of the Saigon confluence with the Dongnai river (Fig 1, triangles). This section of about 90 km in length will be monitored once per orbit from CC to a few kilometers downstream of H1 and twice per orbit on the remaining river reaches up to DN2. The main interest of this study is to understand the potential of SWOT observations to observe instantaneous discharge in a low elevation tidal river given SWOT's expected errors. Hence, the temporal resolution of the SWOT observations is not taken into account.

2.4. Spatial interpolation of in-situ measurements of water level

In order to provide spatial continuity to the data, we chose to employ a quadratic spline interpolation technique. We explored alternative interpolation techniques, including higher-order polynomials and Kriging, but these methods did not yield results as favorable as the second-degree polynomial interpolation (results not presented). The alternative techniques frequently introduced unrealistic characteristics into the water surface due to their increased degrees of

freedom. To define the spatial framework for our interpolation, we used the SWOT River Database (SWORD) [39]. The SWORD database contains the SWOT mission's river vector products for each SWOT overpass, as detailed in the Jet Propulsion Laboratory (JPL) internal document [25]. These vector data products are the definition of SWOT river reaches and nodes for all observable rivers (width $>$ 100 m) in the world. The database provides high-resolution river nodes (200 m) and reaches ($\approx$ 10 km). The 200 meter nodes defined in SWORD for the Saigon river serve as the basis for our spatial interpolation.

The quadratic spline interpolation technique was employed to estimate water levels at unmeasured locations between the in-situ measurement points. This method utilizes a piecewise continuous quadratic polynomial to fit the available data points and provide a smooth representation of the water level distribution along the river. The quadratic spline interpolation relies on the assumption that the river water level between two measurement points can be approximated by a quadratic function. Let's consider a set of in-situ measurements at distinct locations along the river, denoted as (x_i, y_i), where x_i represents the spatial coordinate and y_i represents the measured water level at that point. The quadratic spline interpolant, $I(x)$, between two consecutive data points (x_i, y_i) and (x_{i+1}, y_{i+1}), can be expressed as follows [40]:

$$I(x) = a_i(x - x_i)^2 + b_i(x - x_i) + c_i, \quad \text{for} \quad x_i \leq x \leq x_{i+1} \tag{1}$$

where a_i, b_i, and c_i are the coefficients of the quadratic polynomial determined by solving a system of equations based on the boundary conditions and smoothness constraints. These constraints ensure that the interpolant is continuous and has continuous first derivatives at the data points. Boundary conditions define the behavior of the interpolant at the endpoints of the data points. In our case, we used the natural boundary condition, where the second derivative at the boundary points is set to zero. This condition ensures a smooth and continuous curve throughout the interpolation range. Smoothness constraints impose constraints on the first derivatives of the interpolant at the internal points. These constraints guarantee a smooth transition between adjacent quadratic polynomials and prevent any sudden changes or discontinuities. The quadratic spline interpolation method enforces these constraints, resulting in a physically sound representation of the water level variation along the river's surface. To compute the quadratic spline interpolation, we utilized Python's Scipy library [41]. The library provides a convenient function that automatically determines the parameters for smoothness based on the data distribution. By using these parameters, the spline interpolation adapts to the characteristics of the in-situ measurements, ensuring an optimal balance between smoothness and fidelity to the observed data. The extensive amount of interpolant functions, $I(x)$, results in a considerable number of parameters (a_i, b_i, and c_i) as interpolant functions are computed piece-wise at each 15-minute timestep throughout the 1.5-month period of in-situ measurements (not shown).

To assess the accuracy of the spline interpolation, we employ a framework encompassing three steps: firstly, we evaluate the RMSE and R^2 between the measured and spline time-series, then we compute and compare different tidal metrics, also called datums, that are important for understanding the tidal behavior at each gauge location and its evolution as the tidal wave progresses upstream [42]. Finally, we use wave celerity as a reliable proxy for validation. In a tidal river such as the Saigon River, the tidal wave propagates upstream and is captured by all sensors along the river. The wave celerity is independent of a vertical reference for water level measurements and can serve as a reliable validation parameter for the spline interpolation results. The process of calculating wave celerity involves identifying points where the first derivative of water level measurements is zero at each sensor location. These points, which correspond to the maxima and minima of water levels, are tracked from the downstream to the

upstream sensors to determine travel times. Subsequently, wave celerity in the Saigon river is derived by computing the velocity of these maxima and minima, a procedure that can also be applied to the spline interpolation using the corresponding water level data at sensor locations. A close agreement between the measured and interpolated wave celerities provides confidence in the accuracy of the spline interpolation method to capture the tidal propagation dynamics that govern the water level surface. To contextualize the wave celerity results, we considered several river geomorphological metrics for each river section. Along-river length (L_a), straight-line length (L_s), and sinuosity were quantified to characterize the shape and meandering nature of each river section. Sinuosity is calculated as the ratio of L_a to L_s:

$$\text{Sinuosity} = \frac{L_a}{L_s} \tag{2}$$

This ratio provides a measure of the river's curvature and its deviation from a straight-line course. Rivers can have sinuosity ranging from 1 to 3 (i.e., the river length is three times longer than the valley).

For the period of water level measurements the following metrics were computed according to the general tidal datum computation procedures as described by the US National Oceanic and Atmospheric Administration [43]:

MHHW (Mean Higher-High Water): MHHW is defined as the arithmetic mean of the higher high water heights of the tide observed over a specific period of measurement. Solely, the higher high water of each pair of high waters of a tidal day is included in the mean. It is a reference point for the highest high tides, which occur during spring tides.

MHW (Mean High Water): is defined as the arithmetic mean of all of the high water heights observed over a specific period. It is a reference for the typical height of high tides and is used for navigation, coastal construction, and environmental monitoring.

MRL (Mean River Level): MRL is the average water level over a time period.

MLW (Mean Low Water): is defined as the arithmetic mean of all of the low water heights observed over a specified period and serves as a reference for the typical height of low tides. It is used for navigation, especially in shallow waters.

MLLW (Mean Lower-Low Water): MLLW is defined as the arithmetic mean of the lower low water heights of the tide observed over a specific period. Only the lower low water of each pair of low waters of a tidal day is included in the mean. It serves as a reference point for extremely low tides and is used for coastal planning and environmental monitoring.

Gt (Great Diurnal Range): Gt represents the difference between the mean higher high water (MHHW) and the mean lower low water (MLLW). A larger GT implies a greater difference between high and low tides.

Mn (Mean Range of Tide): Mn is the difference between MHW and MLW. It provides a general measure of the typical tidal variation in a given location.

DHQ (Mean Diurnal High Water Inequality): DHQ is the difference in elevation between MHHW and MHW. It helps assess variations in daily high tide levels.

DLQ (Mean Diurnal Low Water Inequality): DLQ is the difference in elevation between MLLW and MLW. Similar to DHQ, it assesses variations in daily low tide levels.

2.5. Simulation of SWOT satellite products: Water level and slope

In order to conduct an extensive study of error analysis on water level and slope and their impact on discharge estimation using SWOT satellite data we need to simulate these variables. This section outlines the methodology we employed to simulate SWOT water level and slope products.

2.5.1. "True" water level and slope. From the previous section's spline spatial interpolation, we consider the water level obtained as the "true" water level of the river. For the purpose of this study, we focus on the river section around our two sites where ADCP campaigns were done, specifically location H1 and H3 (yellow triangles in Fig 1). However, we will only provide the results for section H1 due to its lower hydraulic complexity compared to location H3, which is located downstream in the center of Ho Chi Minh City. At this location the Saigon river is connected to a complex canal network making the estimation of discharge more challenging. A recent 1D numerical modelling effort has showed that canals influence the dynamics of the river Saigon locally but have negligible influence on the river as a whole [44]. Additionally, at H1 we conducted two ADCP campaigns during both symmetric and asymmetric tidal regimes, allowing us to calibrate our model (to be explained in the next section) based on different tidal types whereas at H3 we only conducted one ADCP campaign.

At the exact location of the ADCP campaign (H1), we consider the spline water level as the true water level, z_{true}. To compute the slope, we select two water level nodes, n_0 and n_N, around H1 with a distance of 1 km between them, as illustrated in green in Fig 2. The true slope, S_{true}, is then calculated using the following equation:

$$S_{true} = \frac{n_N - n_0}{x} \tag{3}$$

with x the along-river distance between the two nodes. This approach allows us to determine the true slope value for our discharge estimation.

To simulate SWOT water level and slope products, we employ two different approaches. Firstly, we aim to obtain the SWOT variables as they are expected to be outputted by the satellite's measurements. Secondly, we propose a new methodology to compute water levels and slope from the SWOT water level products at 200 m resolution.

2.5.2. Approach 1: Expected SWOT products. In this approach, we compute the average water level from the 200 m nodes for the 10 km reach between nodes n_i and n_N as illustrated in red in Fig 2, where N is the total number of water level nodes in the reach and n_i the ith water

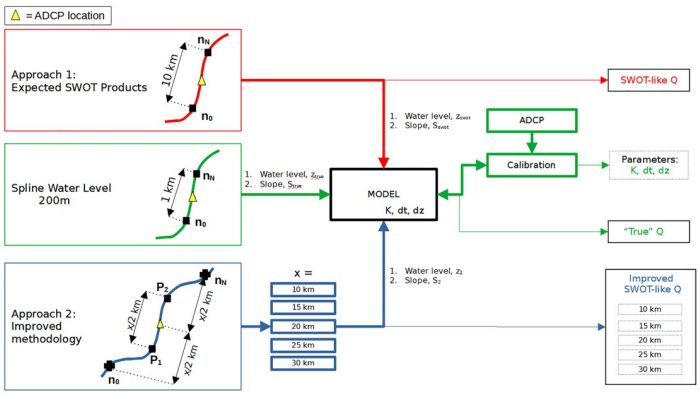

Fig 2. Flowchart of methodology. Flowchart of data used for estimating discharge based on the spline water level (green) to obtain the "True" discharge; based on water level as expected to be provided directly by SWOT (red) to obtain the "SWOT-like" discharge; and based on water level using improved reach selection methodology (blue) to obtain an improved SWOT-like discharge. Discharge is obtained from a modified Manning-Strickler law referred to as the "MODEL" in this flowchart.

https://doi.org/10.1371/journal.pwat.0000226.g002

level node. The SWOT-like water level, z_{swot}, is thus given by:

$$z_{swot} = \frac{1}{N}\sum_{i=0}^{N} n_i \tag{4}$$

The obtained value for z_{swot} mimics the water level product as directly provided by SWOT at the reach scale. We then add the expected noise of 10 cm [12, 45–47] directly to this value. To study the variability of the error, we employ a Monte Carlo white noise approach with standard deviation equal to the expected error and mean equal to zero as has been done in previous studies [22, 36]. For the computation of SWOT-like slope, we follow the methodology proposed by the SWOT team [48] at reach level where the first, n_0, and last node, n_N, of a given reach are used to compute the slope as follows:

$$S_{swot} = \frac{n_N - n_0}{x} \tag{5}$$

where x is the distance spanned by the reach. Similar to the SWOT-like water level, $\bar{Z}_{swot}$, we directly add the expected SWOT error of 1.7 cm/km [12, 45–47] to the computed slope using a Monte Carlo white noise approach. Using this methodology we obtain 1000 samples of SWOT-like water level and slope with associated errors that correspond to the 10 km reach products that will be provided by the SWOT mission.

2.5.3. Approach 2: Improved methodology for water level and slope estimation from SWOT observations. The order of magnitude of the Saigon river's slope (cm/km) is the same as the expected SWOT error's magnitude. Thus, we anticipate that SWOT slope products may introduce significant errors in discharge estimation when used as is. To mitigate this, we propose a new methodology to compute water levels and slope from the SWOT water level product at 200 m resolution, which are expected to have an error of 35 cm [12, 45]. To incorporate this error, we add it to the 200 m nodes of the spline using the Monte Carlo white noise approach as previously described. The water level, z_2, is taken as the average water level between points n_0 and n_N (Fig 2, blue illustration):

$$z_2 = \frac{1}{N}\sum_{i=0}^{N} n_i \tag{6}$$

For the slope computation we take a reach length of x km and compute two supplemental water levels: the first, P_1, is the average of the nodes in the section between point n_0 and the ADCP point (yellow triangle in illustration, Fig 2) with a length of $x/2$ km, and the second is the average of the nodes in the section between the ADCP location and n_N, also with a length of $x/2$ (point P_2). The slope is then computed as follows:

$$S_2 = \frac{P_1 - P_2}{x} \tag{7}$$

We conduct experiments for reach lengths equal to 10, 15, 20 and 25 km. These lengths translate to using 50, 75, 100 and 125 nodes for the water level and slope computations, respectively. By utilizing more information from the SWOT measurements and increasing the number of river nodes used to compute the hydraulic variables we expect a reduction in the error associated with discharge estimation.

The simulated water levels and slopes, obtained through the aforementioned approaches, are utilized to estimate the discharge. The details of the discharge estimation process are explained in the subsequent section.

2.6. River discharge estimation

The instantaneous river discharge was estimated by applying a stage-fall-discharge (SFD) rating curve adapted from the general Manning-Strickler law (Eq 8), previously tested and validated by [49] and used to predict the total discharge of the Saigon river in [20, 30]. The discharge is estimated as follows:

$$Q(t) = \text{sign}(S) \cdot K \cdot A_w(z(t)) \cdot R_h(z(t))^{2/3} \cdot \sqrt{|S(t+\Delta t)|} \quad (8)$$

with Q the water discharge [m^3s^{-1}], K the Manning-Strickler coefficient [$m^{1/3}s^{-1}$], $R_h = A_w/P_w$ the hydraulic radius [m], A_w the wet section [m^2], P_w the wet perimeter [m]. Note that A_w and P_w are both a function of the water level and thus, of time. Furthermore, in Eq 8 above $z(t) = z_{true}(t)$ for computing the "True" discharge, $z(t) = z_{swot}(t)$ for approach 1 and $z(t) = z_2(t)$ for approach 2. The term $sign(S)$ is equal to the sign of the slope, S, taking the values of +1 or -1. The energy slope, S [-], is assumed equal to the water slope and is computed as in sub-sections 2.5.2 and 2.5.3 for approaches 1 and 2, respectively. Since there is no fixed datum between river gauges, we normalize all signals by mean removal, as previously mentioned. This makes the tidal harmonics oscillate about zero for all gauge locations thus, making them comparable. However, datum errors still persist and a vertical adjustment is required for discharge computation. This adjustment is done via an additional term, dz, which serves as an extra tuning parameter of our model and allows it to better capture the surface slope dynamics of the Saigon river. This parameter is introduced in the slope computation as follows:

$$S(t) = s + \frac{dz}{x} \quad (9)$$

where $s = S_{true}$ for computing the "True" discharge, $s = S_{swot}$ for approach 1 and $s = S_2$ for approach 2. In addition, a time lag, Δt, is required to account for the propagation of the tidal wave between the two points used to compute the slope. This method allows the computation of three time-series of discharge namely: the "True" discharge which is used as the benchmark for the discharge computed using approach 1, the SWOT-like discharge, and using approach 2, the improved SWOT-like discharge.

2.7. Performance evaluation indices

The evaluation of the applied approaches was carried out using two statistical indicators: root mean square error (RMSE)and the coefficient of determination (R^2). The RMSE has been evaluated both in terms of absolute (m^3/s) and relative (rRMSE expressed as a percentage) values. These indicators have been widely used in literature for this purpose [36]. Those performance indices have been evaluated referring to the discharge time-series obtained via the Monte Carlo approach for each of the methods described ind section 2.6. The equation, range, and optimal value of each index are presented in Table 1.

Table 1. Equations and optimal values of statistical indices. Q^i and Q^i_{true} denote the predicted discharge from SWOT-like variables and "True" discharge from spline variables, respectively, at time i.

Indices	Equation	Range	Optimal values
Root Mean Square Error	$RMSE = \sqrt{\frac{1}{N}\sum_{i=1}^{N}(Q^i - Q^i_{true})^2}$	0 to ∞	0
Coefficient of determination	$R^2 = 1 - \frac{\sum_i (Q^i_{true} - Q^i)^2}{\sum_i (Q^i_{true} - Q^i_{true})^2}$	0 to 1	1

https://doi.org/10.1371/journal.pwat.0000226.t001

3. Results

3.1. Validation of the spline spatial interpolation

In Fig 3, the time-series from the in-situ water level gauges are shown in the top panel. Six curves are shown for each river gauge from the most downstream (bottom, darker green) to the most upstream (lighter green, top) locations DN2 and CC, respectively. As can be seen, tidal fluctuations govern the water level dynamics at all locations. In fact, the Saigon river's levels are influenced by tides up until the Dau Tieng reservoir (Fig 1) [20]. The panels 0 to 3 illustrate the spatial spline interpolation (black points) and in-situ measurements (triangles) for the four SWOT passes that would occur during the time period of in-situ measurements. For simplicity, we assume that the first pass over the Saigon river (Orbit 1, Day 4, Pass 90) happens on the first day of in-situ measurements. Additionally, the SWOT spatial coverage of the river is indicated in red (pass 90) and blue (pass 271).

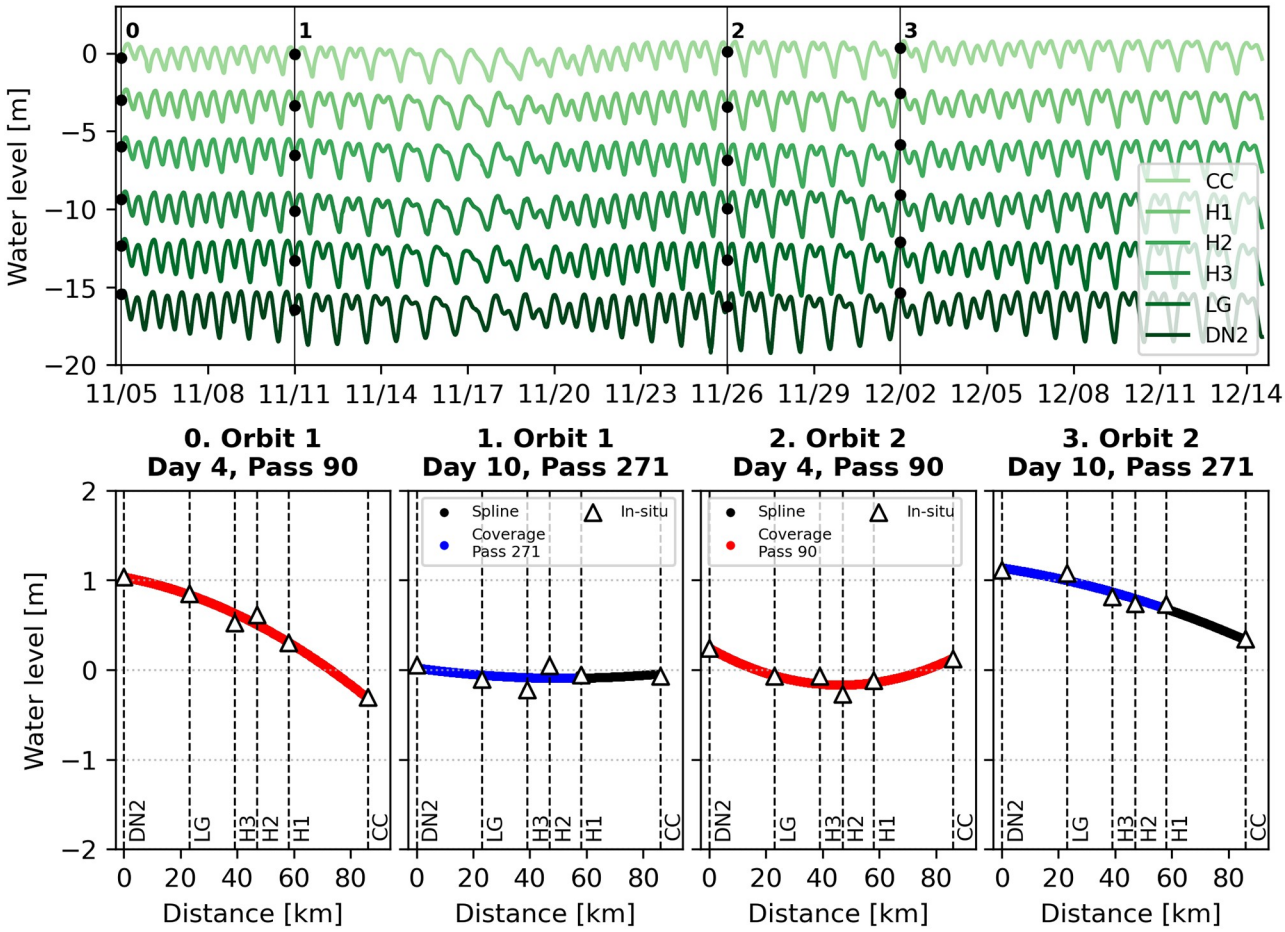

Fig 3. Illustration of spline interpolation and SWOT satellite passes. Time-series from in-situ water level gauges at all locations (top panel). Water levels have been displaced by 3 meters for easier reading. Measurements are shown in increasingly darker shades of green from closest to source to further away from source namely, CC, H1, H2, H3, LG and DN2. Additionally, 4 time stamps corresponding to what would be the SWOT satellite temporal resolution during the period of in-situ measurements are indicated by black, vertical lines. Panels 0 to 3 correspond to the timestamps in the top panel. The results of the spatial interpolation using a second degree spline are illustrated for the SWOT passes over the region namely, pass 90 and 271. Additionally, the SWOT spatial coverage of the river is shown in red (pass 90) and in blue (pass 271). Triangles in panels 0 to 3 indicate in-situ measurements whereas the black dots are the interpolated spline values at the SWORD nodes location.

https://doi.org/10.1371/journal.pwat.0000226.g003

Table 2. Water level Root Mean Square Error (RMSE) and coefficient of determination R^2 at each measurement location. Comparison between the spline fit and in-situ data.

River Location	CC	H1	H2	H3	LG	DN2
RMSE [m]	0.02	0.09	0.10	-0.08	-0.05	0.04
R^2	0.99	0.98	0.96	0.99	0.99	0.99

https://doi.org/10.1371/journal.pwat.0000226.t002

At the DN2 gauge different tidal regimes can be seen propagating upstream. At the beginning of the time-series, a symmetric regime can be seen where different cycles of high and low tide present similar amplitude (Fig 3, from timestamps 0 until November 8th, 2022 in top panel). Then, the tide fluctuations transition to an increasingly asymmetric semi-diurnal regime (timestamp 1) that passes through a diurnal phase (around November 17th, 2022) before cycling back towards a symmetric regime.

From panels 0 to 3 in Fig 3, it can be seen that the quadratic spline fits well to the measured values. From the depicted examples the H3 location seems to be consistently below the spline curve whereas H2 is consistently above. In Table 2, the RMSE and R^2 values for all locations are presented. The results reveal that river measurements at the H2 and H3 locations differ the most from the spline values with, respectively, RMSE of 10 cm and -8 cm. At the other locations RMSE values are below ±10 cm agreeing to the measured values. Additionally, the R^2 values at all locations are above 0.96 which indicates that the spline replicates well the tidal fluctuations along the river.

The tidal metrics are reference water levels describing the characteristic periodic variations in sea surface elevation relative to a vertical datum at a particular location. Table 3 presents tidal metrics for the six gauge locations in meters. For each location, two values are provided in the format "measured, spline." The first value represents the metric computed from measurements (in-situ data), while the second value represents the metric computed from the spline interpolation. The results show consistency in the measured MHHW and MHW values across all locations with values ranging from 0.56 to 1.14 meters and 0.50 to 1.03 meters, respectively. Note that both metrics increase from upstream to downstream within the Saigon river (from CC to LG) and then decrease between the Saigon river (LG) and the Dongnai river (DN2). The spline-based estimates closely align with the measured values, demonstrating the reliability of this method for capturing the tidal dynamics. However, the aforementioned behaviour between the Saigon and Dongnai rivers is not captured by the spline-derived metrics as they monotonically increase from upstream to downstream.

Table 3. Tidal metrics for each gauge location in meters. Two values are shown in the form "measured, spline": the first is the value computed from measurements and the second is the value computed from the spline.

	CC	H1	H2	H3	LG	DN2
MHHW	0.56, 0.56	0.78, 0.79	0.84, 0.88	0.89, 0.85	1.14, 0.98	1.07, 1.06
MHW	0.50, 0.51	0.72, 0.72	0.77, 0.81	0.81, 0.76	1.03, 0.88	0.95, 0.95
MRL	-0.11, -0.11	0.00, 0.02	0.00, 0.05	0.00, -0.04	0.15, 0.00	0.00, 0.00
MLLW	-1.28, -1.28	-1.26, -1.25	-1.37, -1.32	-1.46, -1.49	-1.49, -1.65	-1.80, -1.81
MLW	-0.81, -0.81	-0.79, -0.76	-0.84, -0.78	-0.89, -0.91	-0.83, -0.99	-1.04, -1.03
Gt	1.84, 1.84	2.04, 2.04	2.21, 2.20	2.35, 2.35	2.63, 2.63	2.87, 2.87
Mn	1.31, 1.31	1.51, 1.47	1.61, 1.59	1.69, 1.67	1.86, 1.87	1.99, 1.98
DHQ	0.06, 0.05	0.06, 0.07	0.07, 0.07	0.09, 0.09	0.10, 0.10	0.12, 0.12
DLQ	-0.47, -0.47	-0.47, -0.49	-0.53, -0.54	-0.57, -0.58	-0.66, -0.66	-0.77, -0.77

https://doi.org/10.1371/journal.pwat.0000226.t003

Table 4. Along-river length, L_a, straight-line length, L_s, and sinuosity of each river section between two sensors. Wave celerity is computed for each river section. The "Measured" column refers to the wave celerity computed from measurements and the "Spline" column to wave celerity computed from the spline interpolant. The last row shows the wave celerity for the whole domain.

River section	L_a [km]	L_s [km]	Sinuosity	Measured [m/s]	Spline [m/s]
CC-H1	27.8	16.8	1.65	6.0	5.3
H1-H2	10.5	9.2	1.14	5.6	6.0
H2-H3	8.2	3.8	2.56	6.3	7.3
H3-LG	15.9	5.3	3.00	7.5	6.9
LG-DN2	23.5	13.8	1.70	6.8	6.8
CC-DN2	85.9	48.5	1.77	6.4	6.8

https://doi.org/10.1371/journal.pwat.0000226.t004

MRL values exhibited some variability among locations. The expected measured values for this metric should be around zero which is the case for most stations. However, at the CC station MRL is negative (-0.11 m) and at LG it is positive (0.15 m) potentially due to a measurement bias in the sensors. Spline interpolation provided MRL estimates generally close to zero for all locations. It matched the MRL at the CC station but not at the LG station. This could indicated that the spatial interpolation removed the bias from the measured data at LG as it is located between two other measurement points whereas at CC it could not as it was the last point in the studied river reach.

The results show consistency in the measured MLLW and MLW values across all locations with values ranging from -1.28 to -1.8 meters and -0.81 to -1.04 meters, respectively. As for MHHW and MHW, these metrics increase (in modulus) as we travel downstream but do not show the decrease in value from LG to DN2. The spline-based estimates closely follow the measured values, reinforcing the robustness of the interpolation technique. Other metrics such as Gt, Mn, DHQ and DLQ are computed from MHHW, MHW, MLLW and MLW. As expected these derived metrics show similar characteristics as those discussed and a close agreement between the measured and spline-derived values.

In the Saigon river the tidal wave progresses upstream and is detected by all sensors distributed along the river's course. Wave celerity, a parameter unaffected by the vertical reference of water level measurements, emerges as a dependable means of accessing the capacity of the spline interpolation to propagate the tidal wave. By calculating wave celerity through the use of available in-situ measurements, we can compare it with the wave celerity estimated from the spline-generated water level data. Table 4 presents the wave celerity computed from measured values and from the spline interpolation for river sections between sensor locations.

The results show an average wave celerity along the whole domain of 6.4 m/s based on measured data and 6.8 m/s for the spline interpolation across the domain. Wave celerity values show variability between river sections as these are of different lengths and sinuosity. The most sinuous section is H3-LG with the river being 3 times longer than the straight line course. Overall, the spline is capable of simulating the propagation speed of the tidal wave over the whole domain. However, it seems to have problems in the parts of the river that are most sinuous namely, H2-H3 and H3-LG. This proxy highlights that variations in wave propagation are influenced by the interpolation method and its capacity to capture the timing of high and low waters.

3.2. Calibration of the discharge model using ADCP measurements

Two ADCP (Acoustic Doppler Current Profiler) campaigns were conducted in November 2022 and December 2022, with the utilization of a Rio Grande 600 kHz instrument [50]. Over

a 24-hour period, hourly gauging activities were carried out, encompassing two transects, at locations H1 and H3 (indicated by yellow triangles in Fig 1) using a boat equipped with a georeferenced ADCP device. Nevertheless, the subsequent discussion will focus solely on the H1 location and results for the H3 location can be found in the Figs A-D in S1 Appendix. These ADCP campaigns aimed to calibrate the estimation of water discharge, calculated according to Eq 8 [49]. The methodology followed for calibration was a one-at-a-time procedure that minimizes the RMSE between predicted and observed values. The parameters K, Δt, and dz were adjusted to ensure that the model-derived discharge matched the observed data. Calibration was performed under both symmetric (November 2022) and asymmetric (December 2022) tidal conditions to ensure the robustness of the discharge estimation law. Once calibrated, the parameters are kept constant. In addition, these ADCP campaigns were employed to determine the river's cross-section characteristics and compute Aw and Rh as functions of water level. Considering adverse conditions, ADCP measurement errors were assessed at 10%, with a minimum error threshold set at 100 m^3/s [51]. The optimal results were obtained with a Manning-Strickler coefficient of K = 25 $m^{1/3}/s$, a time step of Δt = -75 minutes, and a vertical resolution of dz = 0.05 meters. Results are depicted in Fig 4. The November 2022 campaign exhibited notably accurate outcomes. In contrast, the December 2022 campaign yielded slightly less precise results but remained in good agreement with the data. The discernible influence of the asymmetric semi-diurnal tidal signal accounted for some of the discrepancies [30]. The discharge time-series for the full period under scope is presented in S1 Fig. The combined RMSE for both campaigns was 450 m^3/s, equivalent to approximately 22% of the maximum observed discharge. Error sensitivity to the calibration parameters was performed and is presented in S2 Fig.

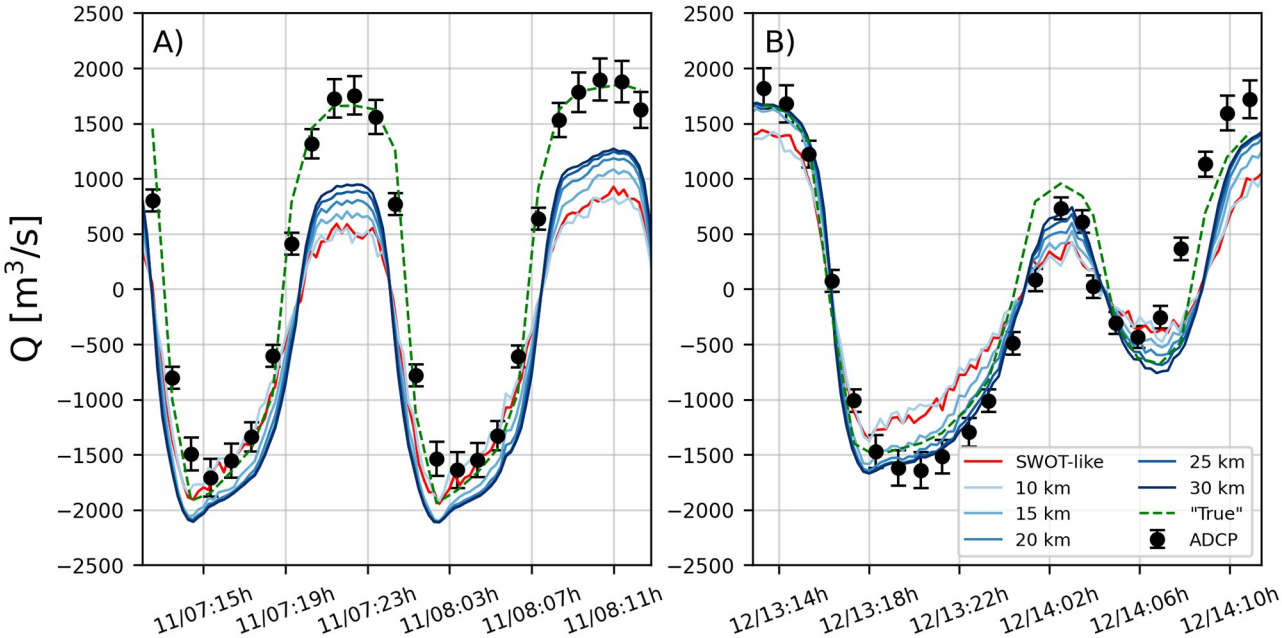

Fig 4. Comparison of river water discharge. Water discharge Q comparison between model results (dashed, green), ADCP measurements (black points), SWOT-like discharge (red) and improved SWOT-like discharge (shades of blue) at the H1 location: (A) symmetric tide during campaigns of November 2022 and (B) asymmetric tide during campaign of December 2022. The curves for SWOT-like discharge and improved SWOT-like discharge are the average of the 1000 Monte Carlo simulations of discharge. All curves were obtained using the optimal parameters namely, $K = 25m^{1/3}/s$, dz = 0.05 meters and dt = −75 minutes.

https://doi.org/10.1371/journal.pwat.0000226.g004

3.3. Discharge estimation using SWOT-like measurements

Fig 5 provides a comprehensive view of the performance and accuracy of SWOT-like discharge estimation techniques based on satellite-derived measurements. In Fig 5A SWOT-like discharge is plotted against the "True" discharge. SWOT-like discharge (red in the figure) is obtained from measurements of water level and slope as SWOT would directly provide and including its expected errors. This estimation of discharge has an R^2 value of 0.31. This signifies a weak correlation between the estimated and "true" discharge values. This discrepancy is particularly noticeable as SWOT-like discharge consistently underestimates true discharge, primarily for higher discharge values (in modulus). Notably, this underestimation is most apparent within the range of positive discharge values spanning from 0 to 1000 m^3/s.

A notable improvement in discharge estimation is introduced through the enhanced SWOT-like discharge estimation methodology, applied to a 10 km reach size (lightest blue in Fig 5A). The resulting R^2 value rises to 0.72, signifying a more robust correlation with true discharge values in comparison to the prior SWOT-like approach. The enhancement is especially evident in cases of negative discharges and positive values exceeding 1000 m^3/s. Nevertheless, we note a persisting underestimation of discharge within the range of 0 to 1000 m^3/s, highlighting ongoing challenges in accurately assessing moderate positive discharge values.

In Fig 5A the effect of varying reach sizes on SWOT-like discharge estimation can be seen with reaches ranging from 15 km to 30 km (increasing shade of blue in figure). As reach size increases, the R^2 value progressively improves, with an improvement from an R^2 of 0.88 at 15 km to 0.94 at 30 km. However, it is essential to acknowledge that this increase in reach size introduces error, leading to a deterioration in discharge estimation accuracy for values between 0 m^3/s and 1000 m^3/s, often yielding negative discharge estimates within this range. Furthermore, the figure shows that beyond a 20 km reach size the improvement in the R^2

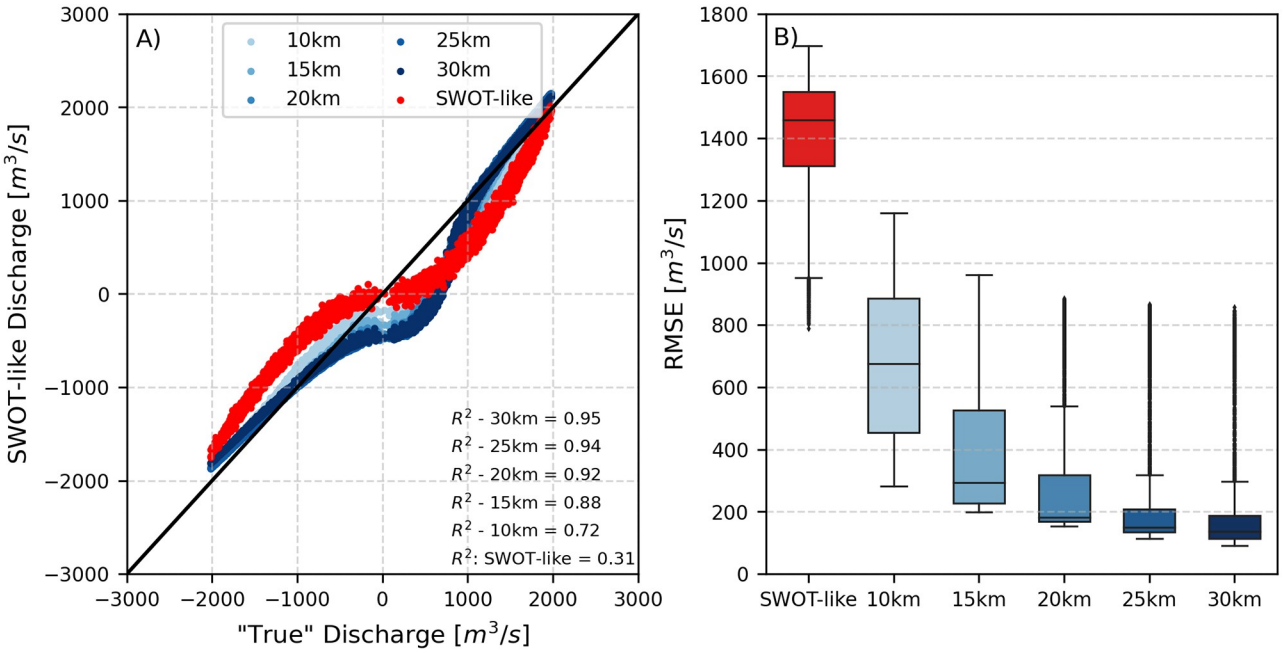

Fig 5. R^2 and RMSE. A) comparison between model discharge taken as "True" discharge, SWOT-like discharge at 10 km reach size and improved SWOT-like discharge at 10, 15, 20, 25 and 30 km reach sizes. Each particle corresponds to the one timestamp in the discharge time-series from each Monte Carlo run. B) RMSE boxplots from Monte Carlo runs between model discharge take as "True" discharge, and SWOT-like discharge at 10 km reach size and improved SWOT-like discharge at 10, 15, 20, 25 and 30 km reach sizes.

https://doi.org/10.1371/journal.pwat.0000226.g005

value becomes less significant. This suggests a diminishing return in accuracy associated with larger reach sizes.

Fig 5B provides a visual representation of the Root Mean Square Error (RMSE) values between the "True" discharge and SWOT-like discharge estimates for a range of Monte Carlo runs. The x-axis comprises six entries, denoting the different methods: SWOT-like (red), 10, 15, 20, 25 and 30 km reaches (shown as increasingly darker shades of blue). Each entry corresponds to a boxplot in the figure, derived from the analysis of time-series from 1000 Monte Carlo runs.

The first box corresponding to SWOT-like discharge estimation exhibits substantial errors across all Monte Carlo runs. The median RMSE for SWOT-like discharge is around 1500 m^3/s (red box in Fig 5B), indicative of a significant discrepancy between the estimated values and the "True" discharge. Moreover, the presence of relatively high outlier RMSEs, reaching values around 800 m^3/s, underscores the variability and extent of errors associated with discharge estimated directly from SWOT measurements in this region. These findings emphasize the limitations of the SWOT satellite and the challenges it presents in accurately approximating "True" discharge values. Conversely, the introduction of the improved SWOT-like methodology with a 10 km reach size results in a enhancement in discharge estimation accuracy. The median RMSE decreases to approximately 700 m^3/s, signifying a considerable improvement in accuracy compared to the SWOT-like approach. Furthermore, the maximum RMSE values remain below 1200 m^3/s, demonstrating a reduced spread in error magnitudes. This marked improvement suggests that the presented methodology for a 10 km reach size is critical in enhancing the precision of discharge estimation from SWOT measurements.

As the reach size increases beyond 10 km, the boxplots in Fig 5B illustrate a trend of diminishing RMSE values. The median RMSE values progressively decrease with larger reach sizes, seemingly reaching a plateau at approximately 180 m^3/s. This plateau suggests that further increases in reach size do not significantly improve the accuracy of discharge estimation, and the methodology approaches a stable level of error. However, it is noteworthy that even at reach sizes between 20 km and 30 km, certain outlier maximum RMSE values remain high at around 800 m^3/s, indicating that challenges persist in accurately estimating discharge for specific Monte Carlo runs. Consequently, a 20 km reach size appears to be an optimal choice for discharge estimation from SWOT measurements, as improvements in median RMSE are not significant with increasing reach size.

Fig 6A presents the relative Root Mean Square Error (rRMSE) values expressed as a percentage (%) between "True" discharge and SWOT-like discharge estimates. These values are shown across the different reach sizes under scope (10 km, 15 km, 20 km, 25 km, and 30 km). Each data point in the figure corresponds to the rRMSE value for a timestamp in the 1000 time-series obtained from the Monte Carlo method, capturing the variability of discharge estimation under different conditions. As can be seen for all estimation methodologies under investigation, the rRMSE values exhibit a trend of increasing error as discharge approaches zero. This trend implies that discharge estimation accuracy diminishes as discharge values approach the lower end of the spectrum.

SWOT-like discharge estimation emerges as the least accurate method, with the highest rRMSE values (red, Fig 6A). The minimum error in discharge is of 50% rRMSE observed at the highest discharge values. This suggests that the SWOT-like methodology struggles to accurately estimate discharge along the full spectrum of discharge values of the Saigon river. Even at the highest discharge values, the rRMSE remains relatively high. Conversely, when implementing the improved SWOT-like methodology with a 10 km reach size (lighter blue particles in Fig 6A), a substantial reduction in rRMSE values is observed. The minimum rRMSE drops to approximately 20% for the largest discharge values, reflecting a considerable enhancement

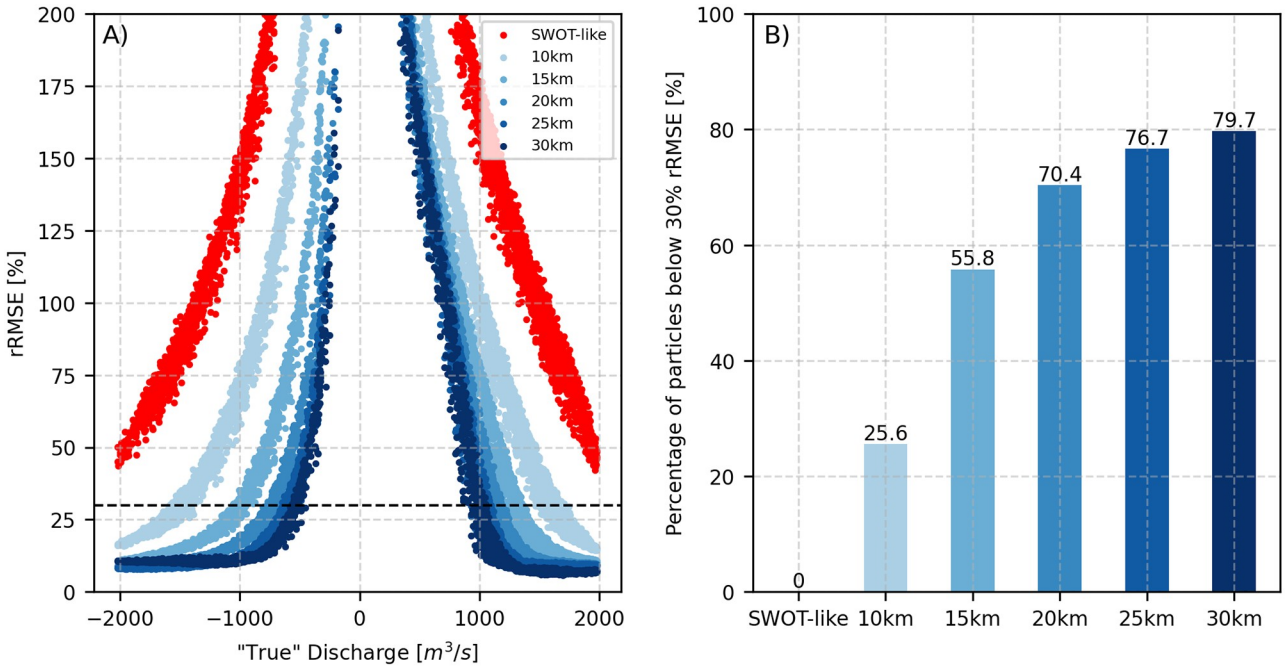

Fig 6. rRMSE. A) rRMSE between model discharge take as "True" discharge, and SWOT-like discharge at 10 km reach size and improved SWOT-like discharge at 10, 15, 20, 25 and 30 km reach sizes. Each particle corresponds to the rRMSE value for a given timestamp in a given Monte Carlo run. The horizontal dashed line represents the 30% rRMSE threshold. B) Bar plot of percentage of Monte Carlo particles below or equal to 30% rRMSE.

https://doi.org/10.1371/journal.pwat.0000226.g006

in accuracy compared to the SWOT-like approach. However, rRMSE values greater than 30% persist for discharge values ranging from -1500 m^3/s to +1500 m^3/s, indicating that challenges in accurate estimation remain within this range.

As in previously seen, the figure demonstrates that increasing the reach size leads to a decrease in rRMSE values. For instance, at a 20 km reach size (indicated by the intermediate blue data points), the minimum rRMSE approaches 10% for the largest discharge values, representing a substantial improvement. Nevertheless, for discharge values between -800 m^3/s and +1200 m^3/s, rRMSE values exceeding 30% are still observed, highlighting the persistence of estimation challenges. Additionally, beyond the 20 km reach size, further increases in reach size do not substantially improve the minimum rRMSE at the largest discharge values. However, these larger reach sizes do result in an increase in the quantity of particles falling below the 30% error threshold. For instance, at a 30 km reach size, discharge values between -600 m^3/s and 1000 m^3/s are still above this threshold. This suggests that while the reach size increase may not substantially enhance accuracy at the highest discharge values, it does contribute to reducing the number of instances where the error exceeds 30% rRMSE.

In Fig 6B the bar plot of the percentage of Monte Carlo particles that are below 30% is shown. As can be seen, we increase the number of particles below this threshold from 0% to 25.6% when applying the improved discharge estimation method for the same reach size. Furthermore, as reach size increases so does the number of particles below the threshold. Increasing reach size from 20 to 30 km increases the number of particles below the 30% rRMSE threshold by 9.3%. Consequently, selecting an appropriate reach size is a crucial consideration for achieving a balance between minimizing error and effectively capturing discharge variability.

In order to study the influence of lower SWOT measurement errors on our discharge estimation methodology, we conducted a sensitivity analysis. The first, publicly available observations of SWOT were remarkably promising, surpassing the SWOT mission team's expectations, and revealing the satellite's impressive ability to discern water nodes in river systems and bodies of water with widths less than 100 meters [13]. Hence, we proceeded to explore the ramifications of reduced SWOT measurement errors. Specifically, we assessed the implications of reducing errors to 30 cm (a 5 cm reduction from the original error) and 25 cm (a 10 cm reduction from the original error) at 200-meter nodes, followed by the application of our methodology under these revised error scenarios. The outcomes of this sensitivity analysis are presented in S3 Fig. We provide comprehensive insights into the rRMSE and the proportion of Monte Carlo particles that fall below the critical 30% rRMSE threshold. Notably, the reduction of SWOT measurement errors to 30 cm yielded a subtle improvement. These improvements were reflected in the percentages of Monte Carlo particles associated with improved SWOT discharge estimates, which ranged from 29.4% to 82% for reaches of 10 to 30 km in length. Similarly, the further reduction to 25 cm in measurement error yielded improved results, demonstrating percentages between 33% and 83.6% of Monte Carlo particles below the 30% rRMSE threshold for various reach sizes spanning from 10 to 30 km. It is important to note that, despite the favorable outcomes observed with the reduced SWOT error scenarios, SWOT-like discharge Monte Carlo particles consistently remained above the specified threshold. However, the overall improvements, albeit notable, remained somewhat limited in magnitude. This restricted enhancement can be attributed to the inherent sensitivity of our simplified discharge estimation model, particularly concerning flow transitions during the shift from positive to negative flow regimes. Consequently, the marginal increment in the number of particles falling below the 30% rRMSE threshold underscores the inherent constraints of our methodology in capturing the intricate dynamics governing tidal flows.

4. Discussion

4.1. Validation of the spline spatial interpolation

It was found that spline interpolation generally fits well with the measured values however, it is noteworthy that the H3 gauge measurements consistently fall below the spline, while H2 gauge values consistently exceed it. This pattern is also reflected in the root mean square error (RMSE) values, which are notably higher at these two locations compared to other gauge locations. This divergence can be attributed to the fact that H3 and H2 stations are situated in an area characterized by high sinuosity (as indicated in Table 4) and an intricate artificial canal network. These two factors exert a significant influence on the propagation of the tidal wave and the hydraulic behavior of the river. Consequently, the spline interpolation encounters challenges in accurately fitting the measurement values at these locations. We also found that the behaviour between the Saigon and Dongnai rivers is not captured by the spline. The spline method is not adapted for simulating adequately discontinuities, such as the confluence between the two rivers.

In contrast, we observed that the spline interpolation aligns well with measurements when considering metrics such as Mean Higher High Water (MHHW), Mean High Water (MHW), Mean Lower Low Water (MLLW), and Mean Low Water (MLW). This consistency suggests that the spatial interpolation method simulates average high and low tides in a coherently over the studied time frame. As anticipated, these metrics, as derived from measurements, exhibit a decline as one moves upstream along the Saigon River, progressing from LG to CC. However, it's worth noting an exception with the DN2 gauge, which shows a decrease in these metrics compared to the LG gauge, even though DN2 is the most downstream measurement location.

This discrepancy arises because DN2 is situated in the Dongnai River, which is considerably wider (by a factor of 3, sometimes more in some regions) and shallower (also by a factor of two) compared to the Saigon River. The spatial interpolation method does not capture this behavior, as it is primarily a mathematical construct.

The use of wave celerity as a proxy to evaluate the spline's ability to propagate the tidal wave yielded promising results across the entire domain. This methodology proved effective in simulating wave celerity. A crucial aspect for discussion pertains to the spatial variability of wave celerity. The spline interpolation performs well in river sections characterized by lower sinuosity (below a value of 2). However, it is evident that the spline-derived wave celerity diverges from measurements within the city center area, where the river exhibits the highest sinuosity, notably between H2 and LG. In the lower reaches of tidal rivers, wave celerity is primarily influenced by friction [1]. Since the spline method represents a mathematical interpolation rather than the physical properties of the water surface, it encounters difficulties in accurately representing wave celerity in highly sinuous sections of the river, leading to either overestimation or underestimation. Moreover, these sinuous areas are often characterized by hydraulic infrastructure and frequent dredging activities, which further contribute to the discrepancies between spline-derived and measured wave celerity values. Dredging, in particular, has a significant impact on this parameter [52].

4.2. Discharge estimation using SWOT-like measurements

SWOT-like discharge obtained from measurements of water level and slope, mirroring the data SWOT satellite would directly provide, demonstrates a relatively weak correlation with "True" values. This observation holds true for both negative and positive discharge values. Notably, an immediate improvement in correlation becomes evident when we implement our new methodology to compute these variables at the same reach size. In fact, the correlation coefficient (R^2) rises to 0.95 for a reach size of 30 km. However, it is noteworthy that as the reach size is increased, the estimation of discharge values within the 0 to 1000 m^3/s range tends to be underestimated compared to SWOT-like discharge (as shown in Fig 5A). This behavior is indicative of the limitations inherent in our discharge estimation method, which relies on the Manning-Strickler law and assumes uniform flow conditions. In situations where the discharge is about to transition from positive to negative or vice versa, uniform flow conditions do not apply, leading to discrepancies. This also elucidates why larger positive and negative values of discharge exhibit a better correlation with "True" values, as flow conditions tend to be closer to uniform when the discharge sign remains constant. Furthermore, as depicted in Fig 4, the mean Monte Carlo profiles for SWOT-like and improved SWOT-like discharge exhibit no temporal discrepancy or time shift. This observation reinforces the notion that the consistent errors mentioned earlier are primarily attributed to the limitations of our discharge estimation model.

Our analysis also revealed that increasing the reach size results in a decrease in discharge RMSE values, eventually reaching as low as 180 m^3/s (as demonstrated in Fig 5B). Nevertheless, it's worth noting that even for larger reach sizes, several outliers persist, with RMSE values reaching up to 800 m^3/s. The presence of these outliers can be attributed to the challenges associated with accurately estimating discharge around zero values, as discussed previously.

Furthermore, our examination revealed that within the range of -500 to +500 m^3/s, the relative RMSE (rRMSE) values surge to more than 200 percent. This phenomenon can be attributed to the same factors discussed earlier. However, it is encouraging to note that our method substantially improves the proportion of Monte Carlo particles that fall below the 30 percent rRMSE threshold, widely considered as satisfactory [9, 53, 54]. The reduction in rRMSE values

can be achieved for discharge values outside the aforementioned range, primarily because we leverage a greater number of SWOT data points for water level. Despite their larger associated errors, the abundance of data points provides more information, which, when averaged, effectively enhances discharge estimation. This aspect is particularly relevant in the context of the Saigon River, given its tidal nature where slope values are of the same order of magnitude as the slope measurement errors provided by SWOT [26].

5. Conclusion

SWOT satellite-based river discharge estimates are poised to offer global discharge information for rivers with widths exceeding 100 meters, encompassing some of the world's largest unmonitored basins. These discharge datasets hold the promise of catalyzing a transformative shift in global hydrological research, contingent on the acceptance of their space-time sampling and associated uncertainties by the global scientific community. The computation of SWOT discharge estimates will rely on relatively straightforward flow laws, which involve the amalgamation of SWOT measurements encompassing water surface elevation (WSE), river width, slope, and parameter estimates related to flow laws.

This study aimed to explore the potential role of the upcoming SWOT satellite data in estimating discharge, a vital variable in various hydraulic and hydrology-related applications. In particular, tidal rivers and their associated floodplains represent critical yet understudied environments that serve as focal points for various human activities and provide habitats for diverse ecosystems. Managing flood risk in these areas is of paramount importance, necessitating comprehensive monitoring and a profound understanding of their hydrological dynamics. In this context, we employed a stage-fall-discharge rating curve derived from the widely recognized Manning-Strickler law [49] to evaluate the potential of SWOT satellite measurements to estimate in real-time water discharge levels in the Saigon-Dongnai River system.

Our analysis focused on a 86-kilometer segment of the Saigon-Dongnai River system in Southern Vietnam, leveraging in-situ water level measurements to obtain a second-degree spline spatial interpolation of the river mimicking that of SWOT (every 200 meters). As the main purpose of this study was to evaluate SWOT-error propagation to discharge estimations as a function of reach size we did not consider the temporal resolution of SWOT data. Furthermore, for low latitude regions the greatest advantage of SWOT is its spatial resolution (river variables at the scale of 10-km reaches or 200-m nodes) rather than its temporal resolution (2 to 3 measurements per month). These simulated measurements were intentionally corrupted with random errors adhering to mission requirements [25]. Especially interesting are the effect of SWOT-derived slope errors on discharge estimates as these are within the same order of magnitude as the Saigon river's slope variations. Subsequently, we estimated discharge values by employing five different river stretch resolutions (equal to 10, 15, 20, 25 and 30 km), following the methodology of [35, 36].

The comparison between synthetic true and SWOT-based discharge at the gauging stations underscores the satellite's potential. The discharge records anticipated from the satellite mission appear capable of providing reliable assessments of the flow regime at various locations. Among the tested discretizations, 20 km stretches exhibited the best performance to computation time ratio, with mean root mean square error (RMSE) values lower than 200 m^3/s and 70.6% of Monte Carlo particles below 30% relative Root Mean Square Error (rRMSE). However, it's imperative to acknowledge that the proposed methodology encounters challenges when estimating discharge values during the transitions between high and low tides, given the non-uniform flow conditions in these situations. Consequently, the estimates are most reliable for high, consistently uniform discharges, whether positive or negative.

Future applications of this research will delve into the potential of spatio-temporal interpolation criteria, such as data assimilation or statistical approaches, which are expected to enhance spatial and temporal coverage of the river network within the mission's constraints (i.e., low revisit time). It's crucial to note that the reliability and completeness of the acquired hydrological information will also hinge on the specific characteristics of the rivers, including discharge variability, seasonality, and more. Rivers with relatively stable discharge patterns are likely to yield more accurate discharge estimations through satellite monitoring. In contrast, rivers characterized by rapid flood waves and high discharge variability may pose challenges for capturing all hydraulic conditions through satellite observation. Subsequent analyses will further investigate these aspects, emphasizing discharge sensitivity to the satellite overpass period and the significance of the river's hydrologic regime. Additionally, since the proposed methodology is independent of the discharge estimation model it can be applied using any other approach for discharge estimation, such as hydraulic numerical models. An effort towards an accurate modelling of the Saigon-Dongnai system is already under way [44].

In conclusion, the methodology put forth to enhance SWOT output and, consequently, improve discharge estimation can be extended to other regions facing data scarcity, hindering continuous monitoring of hydraulic variables. It is crucial to emphasize that in the case of the suggested discharge estimation law it the availability of at least one ADCP campaign at the specific location of interest, and adherence to the assumptions outlined in the proposed model is required.

Supporting information

S1 Appendix. Study at the H3 location.
(PDF)

S1 Fig. Full time-series of discharge at H1 location. Water discharge time-series (green) at the H1 location, residual water discharge time-series obtained from a moving average with a 15 day window size (black) and ADCP campaign (black dots with error bars).
(TIFF)

S2 Fig. Sensitivity analysis of discharge model at the H1 location. Sensitivity analysis of parameters *K*, *dz* and *dt* of the discharge estimation model used in this study at the H1 location.
(TIFF)

S3 Fig. Sensitivity to SWOT error at H1 location. SWOT error of 30 cm (A and B) and 25 cm (C and D) at the 200 meter node level. A) and C): rRMSE between model discharge take as "True" discharge, and SWOT-like discharge at 10 km reach size and improved SWOT-like discharge at 10, 15, 20, 25 and 30 km reach sizes. Each particle corresponds to the rRMSE value for a given timestamp in a given Monte Carlo run. The horizontal dashed line represents the 30% rRMSE threshold. B) and D): Bar plot of percentage of Monte Carlo particles below or equal to 30% rRMSE.
(TIFF)

Acknowledgments

This research was conducted thanks to the financial, technical and human support of the CARE-RESCIF initiative (http://careresCif.hcmut.edu.vn/) within the International Joint Laboratory LECZ-CARE. In addition, we would like to thank Dr. Benoit Camenen for his meaningful input on the first draft of this manuscript.

Author Contributions

Conceptualization: Francisco Rodrigues do Amaral, Tin Nguyen Trung, Nicolas Gratiot.

Data curation: Francisco Rodrigues do Amaral, Tin Nguyen Trung.

Funding acquisition: Thierry Pellarin.

Investigation: Francisco Rodrigues do Amaral, Thierry Pellarin, Tin Nguyen Trung, Tran Anh Tu.

Methodology: Francisco Rodrigues do Amaral.

Project administration: Thierry Pellarin, Tran Anh Tu, Nicolas Gratiot.

Resources: Tin Nguyen Trung, Tran Anh Tu, Nicolas Gratiot.

Supervision: Thierry Pellarin, Tran Anh Tu, Nicolas Gratiot.

Validation: Thierry Pellarin, Nicolas Gratiot.

Visualization: Tin Nguyen Trung.

Writing – original draft: Francisco Rodrigues do Amaral.

Writing – review & editing: Francisco Rodrigues do Amaral.

References

1. Hoitink AJF, Jay DA. Tidal river dynamics: Implications for deltas. Rev Geophys. 2016; 54(1):240–272. https://doi.org/10.1002/2015RG000507
2. Chang FJ, Chen YC. Estuary water-stage forecasting by using radial basis function neural network. J Hydrol. 2003; 270(1):158–166. https://doi.org/10.1016/S0022-1694(02)00289-5
3. Fu LL, Chelton DB. Chapter 2 Large-Scale Ocean Circulation. In: International Geophysics. vol. 69. Cambridge, MA, USA: Academic Press; 2001. p. 133–viii.
4. Stammer C. Satellite Altimetry Over Oceans and Land Surfaces. Andover, England, UK: Taylor & Francis; 2017. Available from: https://www.taylorfrancis.com/books/edit/10.1201/9781315151779/satellite-altimetry-oceans-land-surfaces-detlef-stammer-anny-cazenave.
5. Laignel B, Vignudelli S, Almar R, Becker M, Bentamy A, Benveniste J, et al. Observation of the Coastal Areas, Estuaries and Deltas from Space. Surv Geophys. 2023; p. 1–48. https://doi.org/10.1007/s10712-022-09757-6
6. Arbic BK, Lyard F, Ponte A, Ray RD, Richman JG, Shriver JF, et al. Tides and the SWOT mission: Transition from Science Definition Team to Science Team. PDXScholar. 2015;.
7. Biancamaria S, Lettenmaier DP, Pavelsky TM. The SWOT Mission and Its Capabilities for Land Hydrology. Surv Geophys. 2016; 37(2):307–337. https://doi.org/10.1007/s10712-015-9346-y
8. Gleason CJ, Hamdan AN. Crossing the (watershed) divide: satellite data and the changing politics of international river basins. Geogr J. 2017; 183(1):2–15. https://doi.org/10.1111/geoj.12155
9. Durand M, Gleason CJ, Pavelsky TM, de Moraes Frasson RP, Turmon M, David CH, et al. A Framework for Estimating Global River Discharge From the Surface Water and Ocean Topography Satellite Mission. Water Resour Res. 2023; 59(4):e2021WR031614. https://doi.org/10.1029/2021WR031614
10. Do HX, Gudmundsson L, Leonard M, Westra S. The Global Streamflow Indices and Metadata Archive (GSIM)—Part 1: The production of a daily streamflow archive and metadata. Earth Syst Sci Data. 2018; 10(2):765–785. https://doi.org/10.5194/essd-10-765-2018
11. Gleason CJ, Durand MT. Remote Sensing of River Discharge: A Review and a Framing for the Discipline. Remote Sens. 2020; 12(7):1107. https://doi.org/10.3390/rs12071107
12. Desai S. Surface Water and Ocean Topography Mission (SWOT) Project Science Requirements Document. JPL D-61923, Rev B. 2018;.
13. CNES. SWOT International Science Team Meeting Press Event; 2023. Available from: https://swot.jpl.nasa.gov/resources/206/recording-of-swot-international-science-team-meeting-press-event-september-2023/.
14. IPCC. Climate Change 2023: Synthesis Report. Geneva, Switzerland: The Intergovernmental Panel on Climate Change; 2023.

15. Lossouarn C, Quertamp F, Gratiot N, Fenghua S, Daigo Y. Water Megacities and Global Change: Portraits of 15 Emblematic Cities of the World; 2016. Available from: https://www.researchgate.net/publication/313376505_Water_Megacities_and_Global_Change_Portraits_of_15_Emblematic_Cities_of_the_World.

16. Birkmann J, Garschagen M, Kraas F, Quang N. Adaptive urban governance: new challenges for the second generation of urban adaptation strategies to climate change. Sustainability Sci. 2010; 5(2):185–206. https://doi.org/10.1007/s11625-010-0111-3

17. Fuchs R, Conran M, Louis E. Climate Change and Asia's Coastal Urban Cities: Can they Meet the Challenge? Environment and Urbanization ASIA. 2011; 2(1):13–28. https://doi.org/10.1177/097542531000200103

18. Hanson S, Nicholls R, Ranger N, Hallegatte S, Corfee-Morlot J, Herweijer C, et al. A global ranking of port cities with high exposure to climate extremes. Clim Change. 2011; 104(1):89–111. https://doi.org/10.1007/s10584-010-9977-4

19. Couasnon A, Eilander D, Muis S, Veldkamp TIE, Haigh ID, Wahl T, et al. Measuring compound flood potential from river discharge and storm surge extremes at the global scale. Nat Hazards Earth Syst Sci. 2020; 20(2):489–504. https://doi.org/10.5194/nhess-20-489-2020

20. Rodrigues do Amaral F, Gratiot N, Pellarin T. Assessing typhoon-induced compound flood drivers: a case study in Ho Chi Minh City, Vietnam. Nat. Hazards Earth Syst. Sci. 2023; 23(11):3379–3405. https://doi.org/10.5194/nhess-23-3379-2023

21. Wood M, Haigh ID, Le QQ, Nguyen HN, Tran HB, Darby SE, et al. Climate-induced storminess forces major increases in future storm surge hazard in the South China Sea region. Nat Hazards Earth Syst Sci. 2023; 23(7):2475–2504. https://doi.org/10.5194/nhess-23-2475-2023

22. Durand M, Gleason CJ, Garambois PA, Bjerklie D, Smith LC, Roux H, et al. An intercomparison of remote sensing river discharge estimation algorithms from measurements of river height, width, and slope. Water Resour Res. 2016; 52(6):4527–4549. https://doi.org/10.1002/2015WR018434

23. Simard M, Matte P, Laignel B, Christensen A, Savelli R, Parra AS. SWOT Science and Applications in Deltas and Estuaries: Dealing with Tides. AGU Fall Meeting Abstracts. 2022; 2022:OS22A–31.

24. Srinivasan M, Tsontos V. Satellite Altimetry for Ocean and Coastal Applications: A Review. Remote Sens. 2023; 15(16):3939. https://doi.org/10.3390/rs15163939

25. Stuurman C, Pottier C. Surface Water and Ocean Topography Mission Level 2 KaRIn high rate river single pass vector product; 2020. Available from: https://podaac-tools.jpl.nasa.gov/drive/files/misc/web/misc/swot_mission_docs/pdd/D-56413_SWOT_Product_Description_L2_HR_RiverSP_20200825a.pdf.

26. Fernandez DE. SWOT Project Mission Performance and Error Budget. JPL D-61923, Rev B. 2022;.

27. Nguyen TT, Némery J, Gratiot N, Strady E, Tran VQ, Nguyen AT, et al. Nutrient dynamics and eutrophication assessment in the tropical river system of Saigon—Dongnai (southern Vietnam). Sci Total Environ. 2019; 653:370–383. https://doi.org/10.1016/j.scitotenv.2018.10.319 PMID: 30412882

28. Nguyen AT, Némery J, Gratiot N, Garnier J, Dao TS, Thieu V, et al. Biogeochemical functioning of an urbanized tropical estuary: Implementing the generic C-GEM (reactive transport) model. Sci Total Environ. 2021; 784:147261. https://doi.org/10.1016/j.scitotenv.2021.147261 PMID: 34088067

29. Schwarzer K, Thanh NC, Ricklefs K. Sediment re-deposition in the mangrove environment of Can Gio, Saigon River estuary (Vietnam). J Coast Res. 2016; 75(sp1):138–142. https://doi.org/10.2112/SI75-028.1

30. Camenen B, Gratiot N, Cohard JA, Gard F, Tran VQ, Nguyen AT, et al. Monitoring discharge in a tidal river using water level observations: Application to the Saigon River, Vietnam. Sci Total Environ. 2021; 761:143195. https://doi.org/10.1016/j.scitotenv.2020.143195 PMID: 33189379

31. Nguyen AT, Némery J, Gratiot N, Dao TS, Le TTM, Baduel C, et al. Does eutrophication enhance greenhouse gas emissions in urbanized tropical estuaries? Environ Pollut. 2022; 303:119105. https://doi.org/10.1016/j.envpol.2022.119105 PMID: 35276252

32. Lahens L, Strady E, Kieu-Le TC, Dris R, Boukerma K, Rinnert E, et al. Macroplastic and microplastic contamination assessment of a tropical river (Saigon River, Vietnam) transversed by a developing megacity. Environ Pollut. 2018; 236:661–671. https://doi.org/10.1016/j.envpol.2018.02.005 PMID: 29438952

33. Vachaud G, Quertamp F, Phan TSH, Tran Ngoc TD, Nguyen T, Luu XL, et al. Flood-related risks in Ho Chi Minh City and ways of mitigation. J Hydrol. 2019; 573:1021–1027. https://doi.org/10.1016/j.jhydrol.2018.02.044

34. Rodrigues do Amaral F, Trung TN, Pellarin T, Gratiot N. Datasets of high-resolution water level and discharge from the Saigon-Dong Nai estuary system impacted by a developing megacity, Ho Chi Minh City—Vietnam. Data in Brief. 2023; 48:109147. https://doi.org/10.1016/j.dib.2023.109147 PMID: 37128590

35. de Moraes Frasson RP, Wei R, Durand M, Minear JT, Domeneghetti A, Schumann G, et al. Automated River Reach Definition Strategies: Applications for the Surface Water and Ocean Topography Mission. Water Resour Res. 2017; 53(10):8164–8186. https://doi.org/10.1002/2017WR020887

36. Domeneghetti A, Tarpanelli A, Grimaldi L, Brath A, Schumann G. Flow Duration Curve from Satellite: Potential of a Lifetime SWOT Mission. Remote Sens. 2018; 10(7):1107. https://doi.org/10.3390/rs10071107

37. Fjørtoft R, Gaudin JM, Pourthié N, Lalaurie JC, Mallet A, Nouvel JF, et al. KaRIn on SWOT: Characteristics of Near-Nadir Ka-Band Interferometric SAR Imagery. IEEE Trans Geosci Remote Sens. 2013; 52 (4):2172–2185. https://doi.org/10.1109/TGRS.2013.2258402

38. Nickles C, Beighley E, Zhao Y, Durand M, David C, Lee H. How Does the Unique Space-Time Sampling of the SWOT Mission Influence River Discharge Series Characteristics? Geophys Res Lett. 2019; 46 (14):8154–8161. https://doi.org/10.1029/2019GL083886

39. Altenau EH, Pavelsky TM, Durand MT, Yang X, de Moraes Frasson RP, Bendezu L. The Surface Water and Ocean Topography (SWOT) Mission River Database (SWORD): A Global River Network for Satellite Data Products. Water Resour Res. 2021; 57(7):e2021WR030054. https://doi.org/10.1029/2021WR030054

40. Meir A, Sharma A. Spline Functions and Approximation Theory. Basel, Switzerland: Birkhäuser; 1972. Available from: https://link.springer.com/book/10.1007/978-3-0348-5979-0.

41. Virtanen P, Gommers R, Oliphant TE, Haberland M, Reddy T, Cournapeau D, et al. SciPy 1.0: Fundamental Algorithms for Scientific Computing in Python. Nature Methods. 2020; 17:261–272. https://doi.org/10.1038/s41592-019-0686-2 PMID: 32015543

42. Palmer K, Watson CS, Hunter JR, Hague BS, Power HE. An improved method for computing tidal datums. Coastal Eng. 2023; 184:104354. https://doi.org/10.1016/j.coastaleng.2023.104354

43. NOAA. Computational techniques for tidal datums handbook. NOAA, NOS Center for Operational Oceanographic Products and Services. 2003;.

44. Camenen B, Gerarduzzi K, Terraz T, Rodrigues do Amaral F, Gratiot N, Pellarin T. 1D numerical modelling of a complex tidal river: case of the River Saigon, Vietnam. In: Proc. 7th SimHydro conference; 2023.

45. Peral E, Esteban-Fernandez D. Swot Mission Performance and Error Budget. In: IGARSS 2018—2018 IEEE International Geoscience and Remote Sensing Symposium. IEEE; 2018. p. 8625–8628.

46. Chevalier L, Desroches D, Laignel B, Fjørtoft R, Turki I, Allain D, et al. High-Resolution SWOT Simulations of the Macrotidal Seine Estuary in Different Hydrodynamic Conditions. IEEE Geosci Remote Sens Lett. 2018; 16(1):5–9. https://doi.org/10.1109/LGRS.2018.2862470

47. Tuozzolo S, Lind G, Overstreet B, Mangano J, Fonstad M, Hagemann M, et al. Estimating River Discharge With Swath Altimetry: A Proof of Concept Using AirSWOT Observations. Geophys Res Lett. 2019; 46(3):1459–1466. https://doi.org/10.1029/2018GL080771

48. Stuurman C, Turk F, Fore A, Durand M, Pavelsky T, Frasson R, Williams B, Wei R. SWOT Project Algorithm Theorectical Basis Document. JPL D-105505. Available from: https://archive.podaac.earthdata.nasa.gov/podaac-ops-cumulus-docs/web-misc/swot_mission_docs/atbd/D-105505_SWOT_ATBD_L2_HR_RiverSP_20230713__w-sigs.pdf.

49. Camenen B, Dramais G, Le Coz J, Ho TD, Gratiot N, Piney S. Estimation d'une courbe de tarage hauteur-dénivelée-débit pour une rivière influencée par la marée. La Houille Blanche—Revue internationale de l'eau. 2017; 5:16–21. https://doi.org/10.1051/lhb/2017039

50. Dinehart RL, Burau JR. Repeated surveys by acoustic Doppler current profiler for flow and sediment dynamics in a tidal river. J Hydrol. 2005; 314(1):1–21. https://doi.org/10.1016/j.jhydrol.2005.03.019

51. Le Coz J, Blanquart B, Pobanz K, Dramais G, Pierrefeu G, Hauet A, et al. Estimating the Uncertainty of Streamgauging Techniques Using In Situ Collaborative Interlaboratory Experiments. J Hydraul Eng. 2016; 142(7):04016011. https://doi.org/10.1061/(ASCE)HY.1943-7900.0001109

52. Cai H, Savenije HHG, Yang Q, Ou S, Lei Y. Influence of River Discharge and Dredging on Tidal Wave Propagation: Modaomen Estuary Case. J Hydraul Eng. 2012; 138(10):885–896. https://doi.org/10.1061/(ASCE)HY.1943-7900.0000594

53. Huang Q, Long D, Du M, Han Z, Han P. Daily Continuous River Discharge Estimation for Ungauged Basins Using a Hydrologic Model Calibrated by Satellite Altimetry: Implications for the SWOT Mission. Water Resour Res. 2020; 56(7):e2020WR027309. https://doi.org/10.1029/2020WR027309

54. Du B, Jin T, Liu D, Wang Y, Wu X. Accurate Discharge Estimation Based on River Widths of SWOT and Constrained At-Many-Stations Hydraulic Geometry. Remote Sens. 2023; 15(6):1672. https://doi.org/10.3390/rs15061672